Check for updates

ChemNanoMat

CHEMNANOMAT
CHEMISTRY OF NANOMATERIALS FOR ENERGY, BIOLOGY AND MORE

ACES Asian Chemical Editorial Society

RESEARCH ARTICLE

Surfactant-Free Polyol Synthesis of Effective Pd-Cu Nanomaterials for H_2/O_2 Solid Polymer Electrolyte Fuel Cells

Roberta A. Isidoro[1] | Nihat E. Şahin[2] | Fabio C. Fonseca[1] | Teko W. Napporn[3] | Elisabete I. Santiago[1] | Kouakou Boniface Kokoh[3]

[1]Nuclear and Energy Research Institute, Cidade Universitaria, Sao Paulo, Brazil | [2]Battery and Materials, Department of Biological and Chemical Engineering, Aarhus University, Aarhus N, Denmark | [3]Université de Poitiers, IC2MP, UMR-CNRS 7285, Poitiers cedex 09, France

Correspondence: Nihat E. Şahin (nsahin@bce.au.dk) | Teko W. Napporn (teko.napporn@univ-poitiers.fr) | Elisabete I. Santiago (Elisabete.santiago@usp.br)

Received: 5 June 2025 | **Revised:** 21 October 2025 | **Accepted:** 13 November 2025

Keywords: electrocatalysis | oxygen reduction reaction | Pd-Cu nanomaterials | polyol synthesis | SPE fuel cell

ABSTRACT

This study presents a facile synthesis of carbon-supported binarypalladium-copper (Pd-Cu/C) nanomaterials designed to achieve competitive catalytic activity while reducing material costs in solid polymer electrolyte (SPE) fuel cells. A surfactant-free, microwave-heated polyol process is employed to synthesize Pd/C and Pd-Cu/C nanomaterials with mean particle size below 4.0 nm. The electrocatalytic activity toward oxygen reduction reaction (ORR) and the corresponding kinetic parameters of Pd-Cu/C electrodes with varying compositions are systematically interrogated using rotating disk electrode (RDE) measurements. Notably, Tafel analysis reveals a slope of 60 ± 2 mV per decade slope at low current densities indicating that the first electron transfer to molecular oxygen (O_2) is the rate-determining step. At higher current densities, a slope of 144 ± 8 mV per decade suggests a transition proton-coupled electron transfer as the dominant mechanism. Furthermore, electrochemical performance of membrane-electrode-assemblies (MEAs) reveals a peak power density of ~ 475 mW cm^{-2} with Pd /C cathode under optimal operating conditions. However, increasing the Cu content in the Pd-Cu/C catalysts results in a marked decrease in current density, likely due to partial Cu dissolution. These findings highlight the potential of binary Pd-Cu nanomaterials as promising alternatives to platinum-based catalysts for Pt-free SPE fuel cell applications.

1 | Introduction

The growing demand for developing efficient technologies aimed at improving sustainable energy conversion, particularly in low-temperature solid polymer electrolyte (SPE) fuel cells [1, 2]. However, the scaling-up commercialization of these systems is largely constrained by high-cost and limited durability of electrocatalysts, which are employed in the anodic and cathodic compartments. Although technical advances in the noble metal loading to decrease, for example, the cost of the membrane electrode assembly (MEA) are still progressing, the effectiveness of the cathode catalyst, where the sluggish oxygen reduction reaction (ORR) occurs, needs to be improved [3–6]. Carbon-supported platinum materials are the most used catalyst in both anode and cathode parts for hydrogen oxidation (HOR) or ORRs, respectively [7, 8]. Due to the high price and limited availability of the platinum resources [9], most efforts are focused either on reducing the Pt catalytic loading in a carbon support matrix or adding a nonprecious element as co-catalyst to promote a bifunctional mechanism. In addition, palladium is an alternative catalyst with high catalytic activity to replace platinum in proton exchange membrane (PEM) fuel cells due to their same face-centered cubic (*fcc*) crystal structure and similar atomic size [10–12]. Many efforts were made these last decades to decrease the precious metal (PGM) loadings from some units of mg cm^{-2} to 0.2–0.6 mg cm^{-2} and to 'dilute' the PGM in an inert substrate (20–30% in carbon) [13–15]. At the same period, the introduction of a second metal into the Pd catalyst to form bimetallic nanostructures was observed in the literature to rationally modify the electronic and geometric effects of the electrode

© 2025 Wiley-VCH GmbH.

material and thus to lead to an improvement of the catalytic properties including activity and stability [16–20]. In this respect, researchers devoted considerable effort to improving the performance of low-temperature SPE fuel cells working with either Pd/C or Pd-based materials as catalysts [4, 21, 22]. Especially, Tang et al. [11] demonstrated that Pd/C was an effective cathode for the ORR, enabling a single fuel cell to deliver 508 mW cm^{-2}.

A profound understanding of the relationship between characteristics of nanomaterials and principles of electrocatalysis is the key to designing, tailoring, and synthesis of effective electrode materials. Composition, size, morphology, and thus activity and stability of nanomaterials considerably depend on synthesis routes employed [23–25]. In most synthesis routes require reducing agents, surfactants, and various additives to stabilize the nanomaterials, which impair the simplicity of synthesis steps and create additional costs. The fact that nanomaterials are obtained via several synthesis processes, nonetheless, usage of surfactants and external additives leads to block active sites that facilitate mutual interactions between nanomaterials and electroactive species and thus leads to decreasing activity. Since the pioneering studies in 1986 [26, 27], for nearly 40 years, the utilization of microwave synthesis method has contributed greatly to the preparation of nanomaterials [28–31]. Due to its simplicity and scalability, polyol-assisted synthesis routes are widely employed to prepare nanostructured metal and metal oxide catalysts with controlled size, morphology, and crystallinity [32–35]. Herein, an energy-efficient and surfactant-free microwave-heated polyol synthesis method has been presented, and particular emphasis has efforted to prepare Pd/C and binary Pd-Cu/C nanomaterials to investigate the electrochemical performance in SPE fuel cells. Concerning the durability and degradation various remarkable works reported the impact of operating conditions including operating temperature, applied cell potential, relative gas humidity, and particle migration, particle dissolution, and particle detachment due to carbon support corrosion [36–38]. More recent studies dealing with adverse effects of transition metals such as nickel (Ni), cobalt (Co), iron (Fe), and copper (Cu) on fuel cells have been reviewed [39–41]. However, most of the studies investigated in alkaline mediums, which are beyond practical applications. It is a fact that copper-based catalysts have rarely been reported because of stability issues from a microstructure viewpoint, particularly in acidic medium, which led to adverse effects in catalytic activity. Recently, proton-conducting copper-based metal–organic frameworks (Cu-MOFs) that address the role of stability supporting efficient proton mobility have highlighted with a particular focus on fuel cell applications [42]. Nonetheless, copper-based catalysts as low-cost alternative to platinum group metals have gained growing interest toward low-temperature fuel cells and metal-air batteries [43, 44]. Moreover, corrosion of the carbon support issues arising at high potential cycling overcome by synthesis of robust carbon materials increasing graphitic content [45–47]. Regulating the active sites in catalysts carbon matrix by doping with nitrogen (N), sulfur (S), and phosphorous (P) greatly promises for further optimizing catalytic performance [48, 49].

This study offers both practical and fundamental insights into the synthesis, characterization, and interrogating electrochemical performances of the carbon-supported Pd-Cu nanomaterials in SPE fuel cells. Accordingly, nanomaterials with varying Pd:Cu atomic ratios (90:10, 70:30, and 50:50) were synthesized by one-step, microwave-heated polyol method. Their intrinsic kinetic activities were systematically demystified by rotating disk electrode (RDE) measurements, emphasizing their potential to address the limitations of conventional cathode catalysts. Then after, typical H_2/O_2 single fuel cell tests were conducted using MEA prepared by integrating the synthesized electrocatalyst as cathode, commercial Pt/C as anode, a Nafion-based ionomer suspension, and a proton-conducting membrane.

2 | Results and Discussion

2.1 | Physicochemical Characterization of the Prepared Nanomaterials

Figure 1 demonstrates the X-ray diffraction (XRD) patterns of the as-prepared nanomaterials. The crystalline phases of the Pd/C and Pd-Cu/C materials were identified according to database of the International Centre for Diffraction Data (ICDD). The XRD patterns reveal that the materials exhibit characteristic peaks corresponding to a typical face-centered cubic (fcc) crystal structure, with a space group of *Fm-3m*. A broad observed at about 2θ = 24.4° is attributed to the (002) plane of the graphite, originating from carbon substrate (Vulcan XC-72R) [50, 51]. Moreover, the XRD pattern of Pd/C (Figure 1a) indicates diffraction peaks at 2θ = 39.91°, 46.43°, 68.04°, 81.94°, and 86.47°, which correspond to the (111), (200), (220), (311), and (222) planes of metallic palladium, respectively, confirming the formation of crystalline palladium (ICDD no: 98-005−2251) [31]. Likewise, the diffraction patterns of the $Pd_{90}Cu_{10}$/C, $Pd_{70}Cu_{30}$/C, and $Pd_{50}Cu_{50}$/C materials

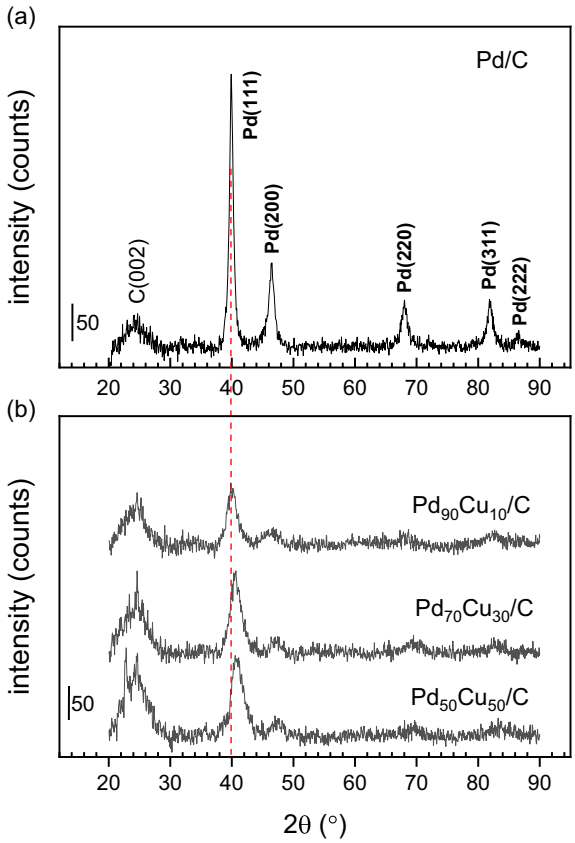

FIGURE 1 | X-ray diffraction patterns of (a) Pd/C and (b) PdCu/C nanomaterials prepared from the one-step microwave-heated polyol method.

2196892x, 2026, 1, Downloaded from https://acces.onlinelibrary.wiley.com/doi/10.1002/cnma.202500324 by University Of Sao Paulo - Brazil, Wiley Online Library on [02/04/2026]. See the Terms and Conditions (https://onlinelibrary.wiley.com/terms-and-conditions) on Wiley Online Library for rules of use; OA articles are governed by the applicable Creative Commons License

(Figure 1b) also depict the characteristic *fcc* structure (ICDD no: 98-010−3082). Notably, a positive shift (about 1.01°) in the Pd(111) is observed from 39.91° in Pd/C to 40.92° in the $Pd_{50}Cu_{50}$(111) sample. This shift is attributed to the substitution of smaller Cu atoms into Pd lattice, suggesting the formation of Pd-Cu solid solutions, as reported elsewhere [52, 53]. No diffraction peaks corresponding to oxide species (PdO, CuO, Cu_2O) were detected in the XRD patterns. The crystallite size, calculated using the five-main diffraction peaks, decreases from 8.9 nm in Pd/C to 7.5 nm in $Pd_{50}Cu_{50}$/C, suggesting that the synthesis procedure employed is effective for promoting alloy formation between Cu and Pd. Considering the (111) diffraction peak, the calculated lattice parameters were 3.9 Å for Pd/C, $Pd_{90}Cu_{10}$/C, $Pd_{70}Cu_{30}$/C, and 3.8 Å for $Pd_{50}Cu_{50}$/C, indicating a progressive incorporation of Cu into the Pd lattice.

Figure 2 displays the X-ray photoelectron spectroscopy (XPS) spectra obtained for the PdCu/C sample. The wide-scan spectrum

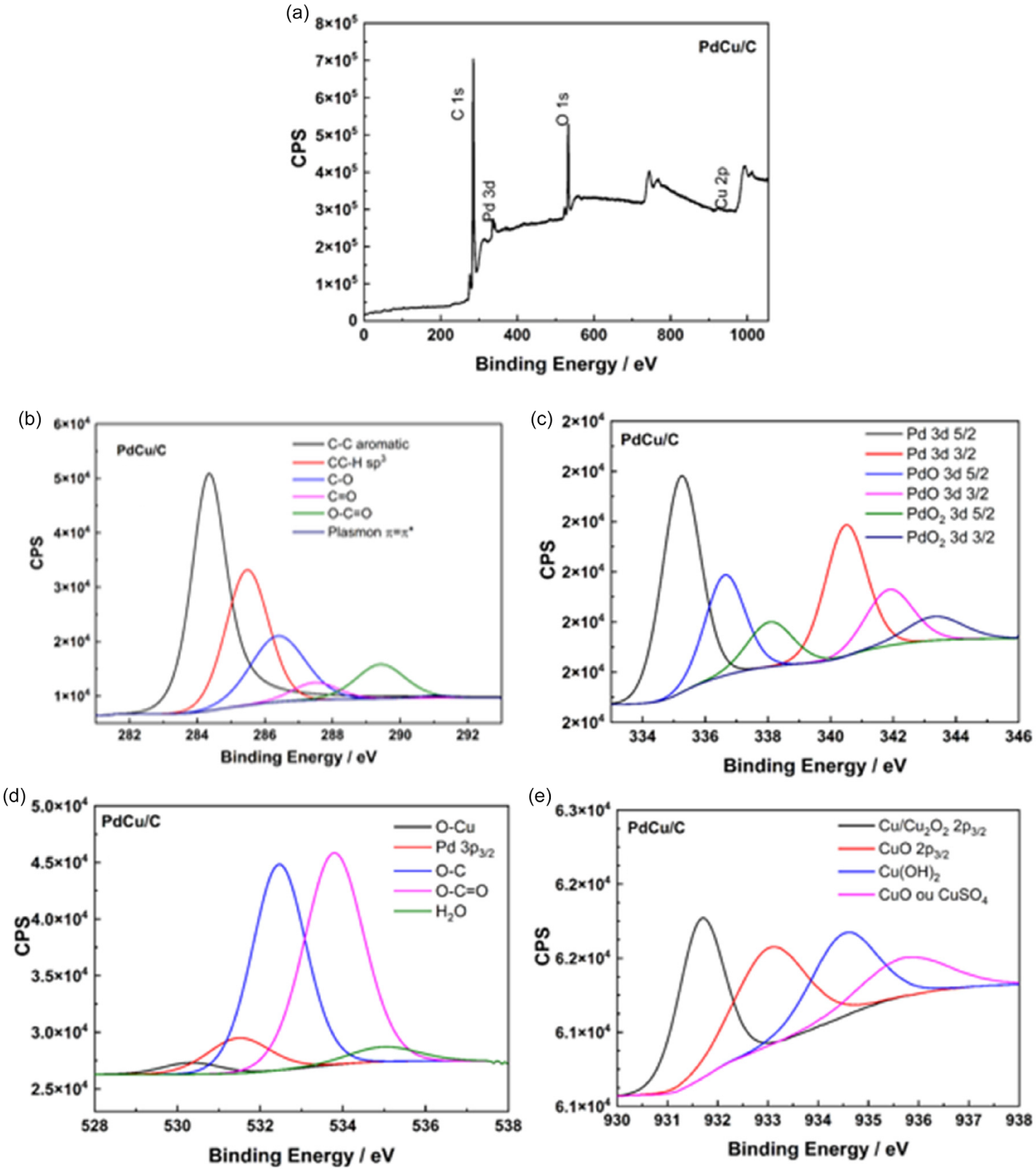

FIGURE 2 | XPS spectra of PdCu/C sample. (a) Wide-scan XPS spectra of PdCu/C, (b) C 1s orbital, (c) Pd 3d orbital, (d) O 1s orbital, and (e) Cu $2p_{3/2}$ orbital.

21996932x, 2026, 1, Downloaded from https://acces.onlinelibrary.wiley.com/doi/10.1002/cnma.202500324 by University Of Sao Paulo - Brazil, Wiley Online Library on [02/04/2026]. See the Terms and Conditions (https://onlinelibrary.wiley.com/terms-and-conditions) on Wiley Online Library for rules of use; OA articles are governed by the applicable Creative Commons License

(Figure 2a) obtained for PdCu/C clearly shows the presence of both Pd and Cu. Meanwhile, the high-resolution C 1s spectrum of the carbon support identifies four distinct chemical environments, as shown in Figure 2b. The dominant peak at 284.4 eV is attributed to aromatic carbon (C–C sp^2), while a secondary component at 285.4 eV corresponds to aliphatic hydrocarbon groups (C–H sp^3), consistently accounting for ≈27% of the total spectral area. Additional contributions from oxidized carbon species include alcohol/ether (C–O, ∼286.5 eV), carbonyl (C=O, 287.5 eV), and carboxyl (O–C=O, ∼289.5 eV) groups. Notably, the incorporation of metals does not significantly alter the relative proportions of these carbon species. The O 1s spectrum (Figure 2d) shows two principal peaks at 532.4 eV and ∼533.7 eV, assigned to oxygen in C–O and O–C=O groups, respectively, in agreement with the C 1s analysis. In samples containing copper (Pd/Cu), an additional low binding energy feature appears at ∼530 eV, indicative of lattice oxygen (O^{2-}) associated with PdO and CuO phases. A weak, high-binding-energy tail suggests the presence of adsorbed molecular water on the nanoparticle surface. Furthermore, the Pd 3d spectrum (Figure 2c) can be deconvoluted into three spin–orbit doublets, each with a fixed splitting of 5.25 eV and an area ratio of 3:2 ($3d_{5/2}$:$3d_{3/2}$). The peak at 335.2 eV (Pd $3d_{5/2}$) corresponds to metallic palladium (Pd^0), while the components at 336.6 eV and ∼338.0 eV are attributed to oxidized Pd species in the form of PdO and PdO_2, respectively. For copper, shown in Figure 2e, the Cu $2p_{3/2}$ spectrum features a main peak at 931.7 eV, which may originate from either metallic Cu or Cu_2O. Additional peaks at 933.0 eV, 934.5 eV, and 935.7 eV correspond to CuO, $Cu(OH)_2$, and $CuSO_4$ species, respectively, indicating the presence of multiple Cu oxidation states on the surface.

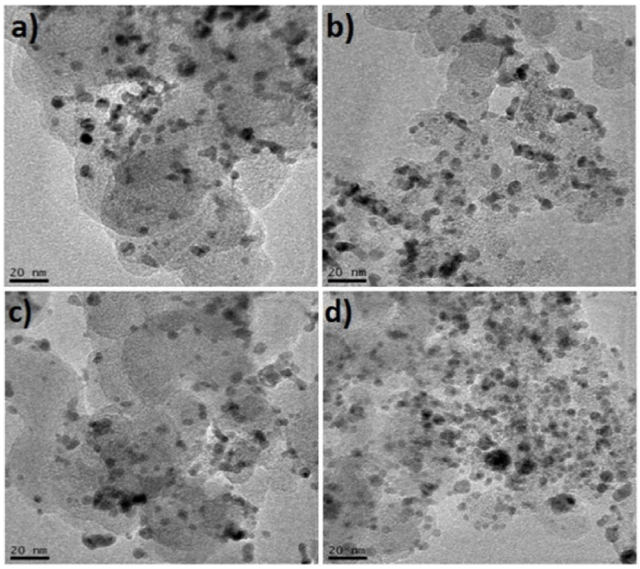

FIGURE 3 | HRTEM micrographs of the (a) Pd/C, (b) $Pd_{90}Cu_{10}$/C, (c) $Pd_{70}Cu_{30}$/C, and (d) $Pd_{50}Cu_{50}$/C nanomaterials recorded at 20 nm scale.

Figure 3 depicts the high-resolution transmission electron microscopy (HRTEM) micrographs, while Figure 4 presents the particle size distribution histograms of the as-prepared materials. The micrographs reveal that the prepared samples exhibit well-dispersed nanoparticles with mean particle sizes of 4.0, 4.0, 3.5, and 3.0 nm for the a) Pd/C, b) $Pd_{90}Cu_{10}$/C, c) $Pd_{70}Cu_{30}$/C, and d) $Pd_{50}Cu_{50}$/C materials, respectively. It is worth noting that the size distributions are relatively narrow, implying a high degree of monodispersed nanoparticles. Also, the micrographs show that the nanoparticles possessed spherical morphology with homogeneous dispersion although slight agglomerations were observed in certain regions. Considering that the smaller particle sizes lead to higher catalytic surface areas (SAs), it is evident that the one-step microwave-heated polyol method produces smaller nanomaterials as compared to those via co-impregnation followed by heat-treatment at 600°C [52].

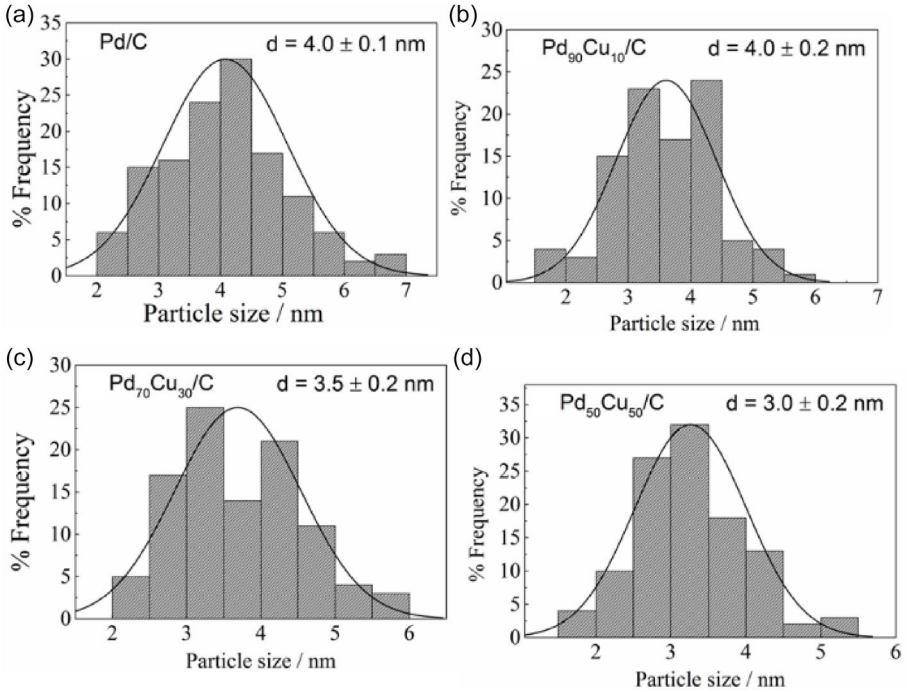

FIGURE 4 | TEM histograms fitted using the log-normal function of the (a) Pd/C, (b) $Pd_{90}Cu_{10}$/C, (c) $Pd_{70}Cu_{30}$/C, and (d) $Pd_{50}Cu_{50}$/C nanomaterials.

21996892x, 2026, 1, Downloaded from https://acces.onlinelibrary.wiley.com/doi/10.1002/cnma.202500324 by University Of Sao Paulo - Brazil, Wiley Online Library on [02/04/2026]. See the Terms and Conditions (https://onlinelibrary.wiley.com/terms-and-conditions) on Wiley Online Library for rules of use; OA articles are governed by the applicable Creative Commons License

2.2 | Electrocatalytic Activity toward the ORR

The electrochemical profile of the prepared nanomaterials is identified by cyclic voltammetry (CV) measurements in N_2-deaerated 0.5 mol L^{-1} H_2SO_4 solution. Accurately determining the open-circuit potential (OCP), where no net current flows and electroactive species are in equilibrium, is essential indicator for evaluating key parameters of the electrochemical reactions expected. As shown in Figure 5a, electrochemical oxidation of Pd to PdO does not occur during the first cycle of CV starting from the OCP value, as expected. To activate the electrode surface and establish reproducible voltammetric behavior between 0.35 V and 1.20 V versus RHE, the Pd/C electrode was subsequently polarized. This treatment facilitates the reversible interconversion of PdO and PdOH species, leading to the formation of a PdO monolayer. During the positive scan, the surface oxidation of electrode starts at about 0.80 V (vs. RHE), as shown in Figure 5a. This oxidation is assigned to the formation of Pd^{2+} species, leading to the development of PdO species. The reduction peak of palladium oxide (PdO) takes place during the backward scan [54]. This peak shifts toward lower potential values depending on the copper content in the material composition (Figure 5b), as recently evidenced by some authors [55, 56]. Furthermore, the lower potential limit was set to 0.35 V (vs. RHE) to prevent the irreversible insertion of hydrogen into the palladium crystal lattice [54, 55]. It is worth noting that to avoid overestimation of the electrode`s active SA, it is essential to limit the potential window during cycling considering electrochemical processes. The SA and electrochemical active SA (EASA) were determined by integrating the reduction peak of PdO, as described elsewhere [56, 57]. The EASA values for Pd/C, $Pd_{90}Cu_{10}$/C, $Pd_{70}Cu_{30}$/C, and $Pd_{50}Cu_{50}$/C nanomaterials were found as 36.0, 35.1, 23.3, and 24.3 m^2 g_{Pd}^{-1}, respectively.

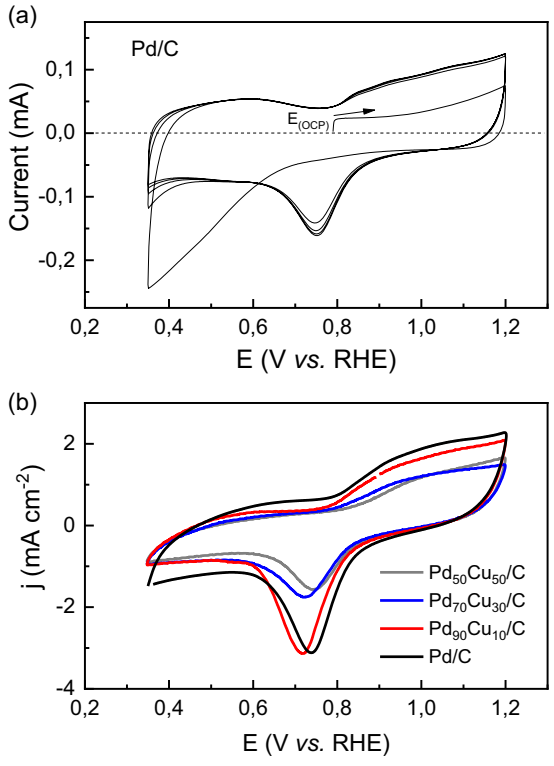

FIGURE 5 | Cyclic voltammograms of (a) Pd/C and (b) Pd-Cu/C nanomaterials recorded at a scan rate of 50 mV s^{-1} in N_2-deaerated 0.5 mol L^{-1} H_2SO_4 supporting electrolyte.

Figure 6 wraps up how to demystify the kinetic parameters through the Koutecký–Levich (K–L) analysis systematically. The ORR polarization curves of the Pd/C electrode are presented in Figure 6a. These curves reveal the presence of three distinct catalytic regions [58, 59]: (i) Activation region, herein at $E > 0.85$ V (vs. RHE), (ii) the mixed kinetic-diffusion control region from *ca.* 0.70 V to 0.85 V (vs. RHE), and (iii) the diffusion limiting current region at E < 0.70 V (vs. RHE). As shown in Figure 6a, the onset potential of the ORR takes place at about 0.88 V (vs. RHE), followed by the appearance of a diffusion-limited plateau extending down to 0.30 V (vs. RHE). With increasing rotational speed, the corresponding limiting currents increase proportionally, indicating enhanced oxygen diffusion toward the electrode surface. Furthermore, the individual contributions of the kinetic and the diffusion currents to the overall measured current were separately evaluated by using K–L equation, as shown in Equation (1) [60]. The K–L equation relates the measured current density (j) to the diffusion-limited current density of O_2 $|j_L^{diff}|$in the bulk electrolyte, as defined by Levich in Equation (2), and the apparent kinetic current density of the ORR $|j_k^{app}|$ at the overpotential (η), as expressed in Equation (3).

$$\frac{1}{|j|} = \frac{1}{|j_L^{diff}|} + \frac{1}{|j_k^{app}|} \tag{1}$$

$$j_L^{diff} = 0.201 n F \left(D_{O_2}\right)^{\frac{2}{3}} C_{O_2} \nu^{-\frac{1}{6}} \omega^{\frac{1}{2}} \tag{2}$$

The coefficient 0.201 is used when the angular velocity (ω) is expressed as the rotation rate of electrode in revolutions per minute (rpm). In this context: n is the number of electrons transferred per reduced oxygen molecule, F is the Faraday constant (96,485 C mol^{-1}), (D) is the diffusion coefficient of oxygen (2.01×10^{-5} cm^2 s^{-1}), (C) is the bulk concentration of dissolved oxygen (1.03×10^{-3} mol L^{-1}); ν is the kinematic viscosity of the electrolyte (1.07×10^{-2} cm^2 s^{-1}) [8, 61].

$$\frac{1}{j_k^{app}} = \frac{1}{j_L} + \frac{1}{j_0}\left(\frac{\theta}{\theta_{eq}}\right) \exp\left(\frac{|\eta|}{b}\right) \tag{3}$$

where j_L is the diffusion-limiting current density being the key phenomenon of the O_2 mass transport, depending on the catalytic film thickness [62]. j_0 (mA cm^{-2}) represents the exchange current density that is the net current passed at the equilibrium potential $E_{eq} = 1.185$ V (vs. RHE) in 0.5 M H_2SO_4 electrolyte [63]. θ and θ_e represent the fractional surface coverage of the electrode by assuming oxygen adsorption at the applied potential (E) and the equilibrium potential (E_{eq}), respectively.

The K–L plots (Figure 6b) were constructed by plotting the inverse of the measured current density as a function of the inverse square root of the electrode rotation rate at different potentials. The linear and parallel behavior of these plots across all potentials indicates that the ORR follows first-order kinetics. To evaluate the contribution of the limiting current density, the $|j_k^{app}|$ values were first calculated from the intercepts of the K–L plots based on Equations (1) and (2). Subsequently, plotting $1/|j_k^{app}|$ as a function of the electrode potential (Figure 6c) enables the determination of the main limiting current density (j_L), as described in Equation (4).

21996892x, 2026, 1, Downloaded from https://acces.onlinelibrary.wiley.com/doi/10.1002/cnma.202500324 by University Of Sao Paulo - Brazil, Wiley Online Library on [02/04/2026]. See the Terms and Conditions (https://onlinelibrary.wiley.com/terms-and-conditions) on Wiley Online Library for rules of use; OA articles are governed by the applicable Creative Commons License

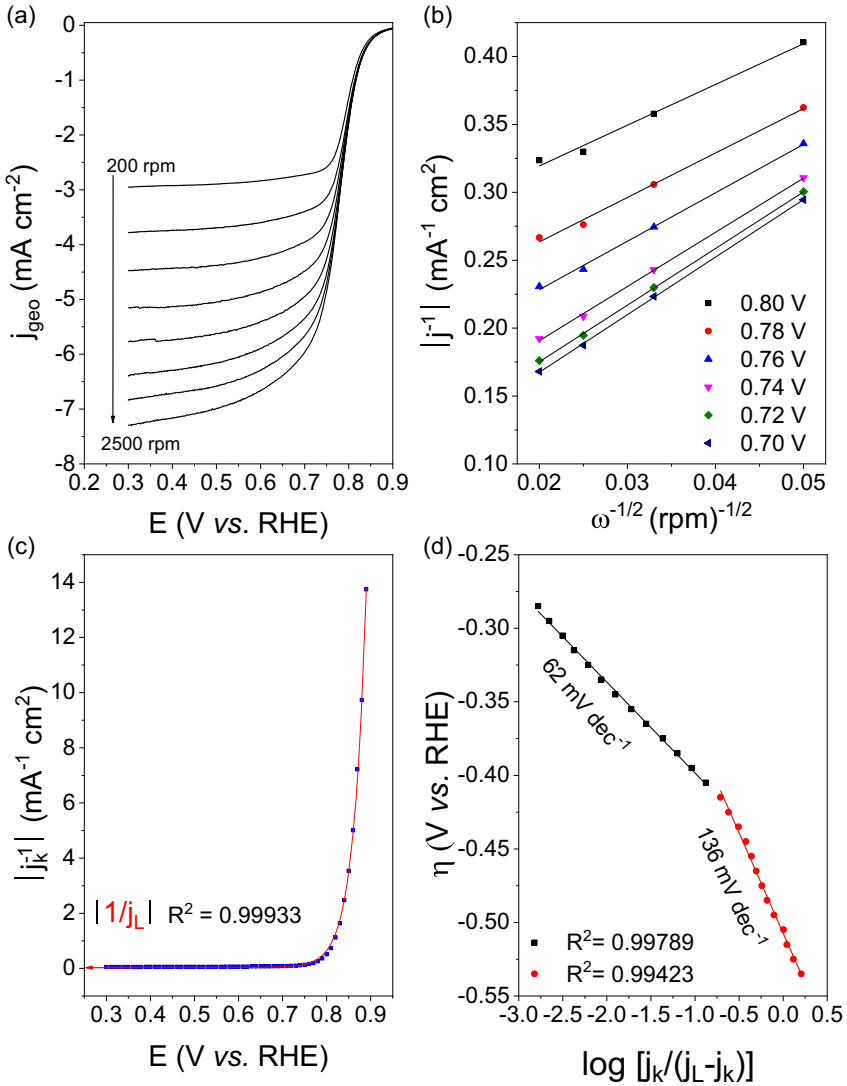

FIGURE 6 | (a) Polarization curves of the Pd/C recorded at different rotation rates with a scan rate of 5 mV s^{-1} in an O_2-saturated 0.5 M H_2SO_4 electrolyte, (b) related Koutecký–Levich plots determined at different potentials from 0.80 to 0.70 V vs. RHE, (c) Plot of $1/j_k$ as a function of the applied potential, and (d) related Tafel plots for low over potential and high over potential regions. The total metal loading on the electrode: 51 μg cm^{-2}.

$$\frac{1}{j_L} = \frac{1}{j_L^{ads}} + \frac{1}{j_L^{film}} \quad (4)$$

The main limiting currents of the ORR were determined from the extrapolated K–L plots and summarized in Table 1. Additionally, the specific kinetic current densities (j_k) were assessed by normalizing the kinetic current at 0.80 V versus RHE with either the SA (in cm^2) or EASA (in mg$^{-1}{}_{Pd}$) values. Tafel plots for the ORR, shown in Figure 6d, were constructed using Equation (5), and display two distinct linear regions. These regions exhibit different Tafel slopes, which increase gradually as applied potential decreases, consistent with a change in the rate-determining step [64].

$$\eta = E - E_{eq} = -b\left[\ln\frac{j_L}{j_0} + + \ln\left(\frac{j_k^{app}}{j_L - j_k^{app}}\right)\right] \quad (5)$$

The Tafel slopes of 62 and 136 mV dec^{-1} are consistent with values typically reported for the ORR on Pd-based catalysts

TABLE 1 | Kinetic parameters for oxygen reduction reaction on the prepared electrodes.

Catalyst	*n*	$j_{k,(SA)}$ @ 0.80 V, mA cm^{-2}	$j_{k,(EASA)}$ @ 0.80 V, mA mg$^{-1}{}_{Pd}$	j_L, mA cm^{-2}
Pd/C	3.96	0.107	3.84	33
$Pd_{90}Cu_{10}$/C	3.95	0.132	4.63	30
$Pd_{70}Cu_{30}$/C	3.91	0.248	5.77	35
$Pd_{50}Cu_{50}$/C	3.90	0.290	7.03	32

2199692x, 2026, 1, Downloaded from https://acces.onlinelibrary.wiley.com/doi/10.1002/cnma.202500324 by University Of Sao Paulo - Brazil, Wiley Online Library on [02/04/2026]. See the Terms and Conditions (https://onlinelibrary.wiley.com/terms-and-conditions) on Wiley Online Library for rules of use; OA articles are governed by the applicable Creative Commons License

[16, 21, 65] and likely correspond to Temkin and Langmuir adsorption isotherms, respectively. Furthermore, the number of electrons transferred per oxygen molecule was found to be close to 4, as listed in Table 1, indicating a predominantly four-electron reduction pathway. The key kinetic parameters, including the exchange current density (j_0) and Tafel slopes, are summarized in Table 2. The polarization curves and corresponding K–L plots for the Pd-Cu cathodes are depicted in Figs. S1-S3 in the Supplementary Information.

2.3 | Performance of the Catalysts in a Single H_2/O_2 Fuel Cell

The fuel cell measurements of Pd/C and Pd-Cu/C nanomaterials as cathode catalysts and a commercial Pt/C as anode catalyst with the same metal loading (0.4 mg cm^{-2}) were carried out at the temperature of 80°C. Figure 7 compares the polarization and power density curves of as-prepared catalysts. As shown, the open circuit voltage (OCV) remains within the range of 0.85 – 0.90 V for all cathode compositions, suggesting a similar electrochemical reaction across the tests. However, the maximum power density, which reaches 475 mW cm^{-2} for Pd/C, decreases to 302 mW cm^{-2} as the Cu content in the Pd-Cu/C catalyst increases to 50 %. This decline may stem from modification of the electronic structure of Pd upon Cu incorporation, which may reduce the number of active sites and thereby decrease overall catalytic activity. It is significant to mention that direct comparison with fuel cell performances reported in the literature is scarce due to differences in experimental parameters such as the type of membrane used (Nafion 117 in Ref. [4]), metal loading [66], and material synthetic method [67]. For a more insightful comparison, Table 3 summarizes the fuel cell performance metrics of Pd/C and binary PdCu/C as well as Pt/C [68] catalysts tested under comparable operating conditions.

Conversely to the positive electronic effect obtained with some transition metals such as Ag and Ni when alloyed with Pd, copper does not seem to promote a beneficial effect with a large amount. This negative effect can be observed on Figure 7b, where increasing the Cu content in the Pd-based cathode results in a decrease in current density. This phenomenon can be explained by a mechanism previously proposed by Fouda-Onana et al. [69], which consists of an associative electrochemical adsorption of the intermediate OOH_{ads}, followed by dissociative recombination on the Pd-Cu bimetallic surface. Accordingly, the ORR on the Pd-Cu proceeds via the following rate-determining step:

$$\text{Pd–Cu(OOH)}_{ads} \rightarrow \text{PdO}_{ads}\text{Cu(OH)}_{ads} \quad (6)$$

Subsequently, a high Cu content in the Pd-Cu cathode induces decrease in the number of electrons transferred per oxygen

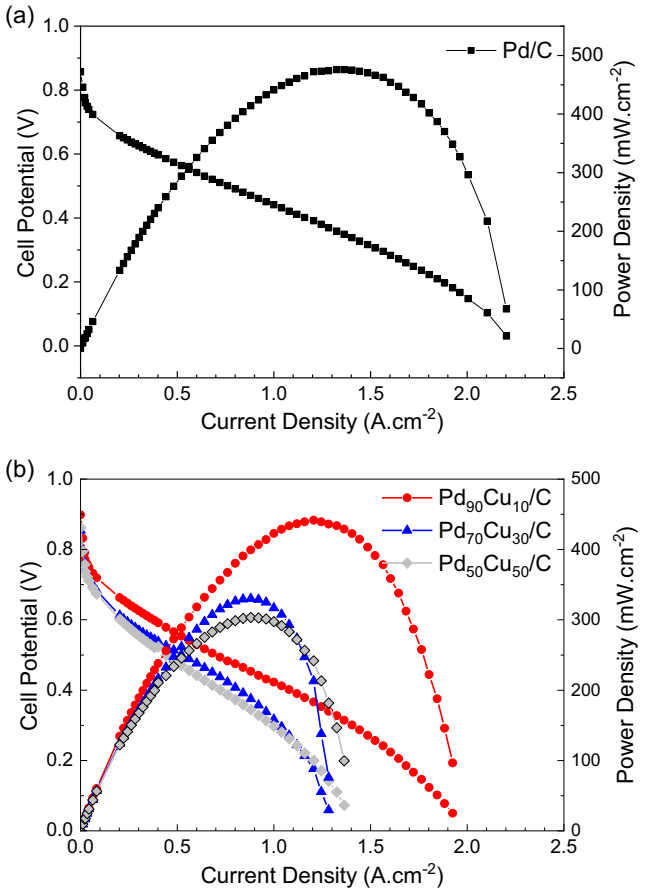

FIGURE 7 | Electrical performance of a 5 cm^2 single H_2/O_2 SPE fuel cell operating at 80°C with Nafion-115 membrane: Pt/C (0.4 mg cm^{-2})/H_2 humidified at 95°C//O_2 humidified at 85°C/Cathode (0.4 mg_{Pd} cm^{-2}). (a) Pd/C as cathode; (b) Pd_xCu_{100-x}/C as cathode. All data were performed at atmospheric pressure.

molecule, which suggests a higher formation of intermediates, such as hydrogen peroxide. On the other hand, according to *d*-band theory, this observation is consistent with recent theoretical and experimental studies, which highlight that tuning *d–d* orbital hybridization can effectively modulate the electronic structure of bimetallic systems and, consequently, govern their catalytic functionality [70, 71]. In particular, in the Pd-Cu bimetallic system, the *d–d* orbital hybridization brings about a shift in the d-band center of Pd, resulting from electronic interactions with Cu, which has a lower electronegativity. This shift tends to weaken the adsorption strength of reaction intermediates, thereby influencing both the activity and selectivity of catalysts during electrochemical processes. While Pd alone is highly active for catalytic reactions, it suffers from strong binding to poisons, which can limit performance. Briefly, in bimetallic Pd-Cu systems, Pd possesses a filled 4d shell with its

TABLE 2 | Tafel slope and exchange current density for oxygen reduction reaction on the prepared electrodes.

Catalyst	*b*, *mV dec*$^{-1}$	j_0, A cm^{-2}	*b*, *mV dec*$^{-1}$	j_0, A cm^{-2}
Pd/C	62	2.10×10^{-8}	136	1.58×10^{-5}
$Pd_{90}Cu_{10}$/C	60	2.10×10^{-9}	153	2.79×10^{-6}
$Pd_{70}Cu_{30}$/C	61	2.10×10^{-9}	140	2.18×10^{-6}
$Pd_{50}Cu_{50}$/C	57	2.10×10^{-9}	149	2.89×10^{-6}

2199692x, 2026, 1, Downloaded from https://acces.onlinelibrary.wiley.com/doi/10.1002/cnma.202500324 by University Of Sao Paulo - Brazil, Wiley Online Library on [02/04/2026]. See the Terms and Conditions (https://onlinelibrary.wiley.com/terms-and-conditions) on Wiley Online Library for rules of use; OA articles are governed by the applicable Creative Commons License

TABLE 3 | Comparison of PEM fuel cell performance at different operating conditions.

Cathode material	Anode material	Membrane	Open circuit voltage, mV	MEA-operated temperature, °C	Power density, mW cm^{-2}	Ref.
Pd/C 0.4 mg cm^{-2}	Pt/C 0.4 mg cm^{-2}	Nafion-115	860	80	475	Here
$Pd_{90}Cu_{10}$/C 0.4 mg cm^{-2}	Pt/C 0.4 mg cm^{-2}	Nafion-115	900	80	440	Here
$Pd_{70}Cu_{30}$/C 0.4 mg cm^{-2}	Pt/C 0.4 mg cm^{-2}	Nafion-115	850	80	330	Here
$Pd_{50}Cu_{50}$/C 0.4 mg cm^{-2}	Pt/C 0.4 mg cm^{-2}	Nafion-115	860	80	302	Here
PdCu/C 0.14 mg cm^{-2}	Pt/C 0.8 mg cm^{-2}	Nafion-117	900	80	150	[4]
Pd/C 0.4 mg cm^{-2}	Pt/C 0.4 mg cm^{-2}	Nafion-115	800	70	330	[67]
Pt/C 0.4 mg cm^{-2}	Pt/C 0.4 mg cm^{-2}	Nafion-112	900	70	669	[68]

d-band center located near Fermi level, whereas Cu has filled 3d configuration. The incorporation of Cu leads to downward shift in the d-band center of Pd, primarily due to electron donation from Cu 3d orbitals to the Pd 4d orbitals [72–74]. This electronic modification results in weaker adsorption of reaction intermediates on Pd active sites. Indeed, this modification can be beneficial in reaction where strong adsorption impedes catalytic performance. This type of electronic interaction has been widely studied in catalysis such as hydrogenation [75, 76], CO oxidation [77, 78], and electrochemical alcohol oxidation [79]. In our study, as shown in Figure 7b, excessive incorporation of Cu may diminish the number of active Pd sites, thereby negatively affecting the overall catalytic performance.

3 | Conclusion

The development and microstructural characterization of Pd/C and binary PdCu/C nanomaterials serving as cathode catalysts have been efforted. In this regard, a surfactant-free microwave-heated polyol method was employed without the use of an additional reducing agent. The observed shift in XRD peak positions for PdCu/C relative to the Pd/C confirms the formation of Pd-Cu alloys, attributed to the incorporation of Cu atoms into the Pd lattice, thus validating the effectiveness of synthesis protocol. The RDE measurements for the ORR, combined K–L analysis, enabled accurate determination of kinetic parameters. The ORR was found to proceed predominantly via a four-electron transfer pathway. However, the number of transferred electrons slightly decreased with increasing the copper content, feasibly due to partial Cu dissolution under operating conditions, which may cause a reduction in catalytic activity. It is observed that maximum performance reached about 475 mW cm^{-2} with Pd/C as the cathode, while it slightly reduced by the increase of the Cu content in the Pd-Cu material composition. Nonetheless, PdCu/C catalysts exhibited notable ORR activity while reducing noble metal content, which is essential for integrating low-cost catalysts into long-term operation. These findings highlight the promising potential of Pd-based materials as Pt-free cathode catalysts for SPE fuel cell applications under realistic operating conditions.

4 | Experimental Section

4.1 | Synthesis of the Electrode Nanomaterials

Carbon-supportedpalladium Pd/C and binary $Pd_{90}Cu_{10}$/C, $Pd_{70}Cu_{30}$/C, and $Pd_{50}Cu_{50}$/C nanomaterials are prepared by reduction of potassium tetrachloropalladate (II) (Alfa Aesar, 99.99%) and copper (II) chloride (Alfa Aesar, 98%), using one-step microwave-heated polyol method under continuous N_2 flow. The synthesis of Pd/C process is detailed elsewhere [39], and described as follows: a required amount of K_2PdCl_4 (0.18 mmol) is dissolved in 100 mL of ethylene glycol (EG, CH_2OH-CH_2OH) under constant ultrasonication for 5 min. Then, the pH value of the solution is gently adjusted to 11 by dropping NaOH (2.0 mmol) prepared in the EG under stirring. Afterward, to yield a metal loading of 20 wt.%, the required amount of pre-treated Vulcan XC-72R carbon black (80 mg) is added under stirring at 1000 rpm for 15 min. The mixture is then placed in the microwave oven (CEM, Synthesis Technology Inside) and operated at 180°C with a power output of 800 W for 30 min. Finally, the resulting suspensions are filtered on a 0.22 μm GSWP (Fisher-Bioblock paper), rinsed with 500 mL of ultrapure water, and dried in an oven at 60°C for 12 h. To synthesize the binary PdCu/C nanomaterials, the similar process is employed by introducing a required amount of $CuCl_2$ beside that of K_2PdCl_4 in 100 mL of EG.

4.2 | Physicochemical Characterization of the Electrode Materials

The XRD patterns of the prepared materials are measured with a Rigaku Multiflex diffractometer including a copper tube powered at 45 kV and 40 mA ($Cu_{,K\alpha1}$ = 1.54060 Å and $Cu_{,K\alpha2}$ = 1.54443 Å). To avoid interference from the kβ component, a nickel filter is installed in a secondary optic. Each XRD pattern is investigated from 20 to 90° in step mode, with 0.05° and fixed acquisition time of 2 min/step. The width of the (111) peak is used to calculate the crystallite size and lattice parameter of the nanoparticles according to Scherer's equation [80] and the Bragg formula [81], respectively. International Center for Diffraction Data (ICDD), Powder Diffraction File (PDF) served as the reference database for phase identification. XPS analysis was performed using a commercial UNI-SPECS UHV system (Berlin, Germany) under an operating pressure below 5×10^{-7} Pa. The Mg Kα line ($h\nu$ = 1253.6 eV) was used as the ionization source, and the analyzer pass energy was set to 10 eV. The inelastic background of the high-resolution spectra for Pd 3d, Ag 3d, Cu 2p, Ni 2p, C 1s, and O 1s was subtracted using the Shirley method. Surface composition (at.%) within the top ~ 5 nm was calculated from the relative peak areas, corrected using Scofield atomic sensitivity factors, with an accuracy of ±5%. The binding energies were calibrated by setting the hydrocarbon C 1s peak to 285.0 eV. Spectral deconvolution was performed using a Voigt-type function composed of 70%

2199692x, 2026, 1, Downloaded from https://acsjournals.onlinelibrary.wiley.com/doi/10.1002/cnma.202500324 by University Of Sao Paulo - Brazil, Wiley Online Library on [02/04/2026]. See the Terms and Conditions (https://onlinelibrary.wiley.com/terms-and-conditions) on Wiley Online Library for rules of use; OA articles are governed by the applicable Creative Commons License

Gaussian and 30% Lorentzian contributions. The full width at half maximum (FWHM) ranged from 1.1 to 2.1 eV, and peak positions were determined with a precision of ±0.1 eV. The morphological observation of the as-prepared nanoparticles is characterized by HRTEM. The measurements are carried out using a JEOL JEM-2100 electron microscope operated at 200 kV accelerating voltage. The samples are prepared from specific amount of catalyst powder stirred in ethanol and then a few drops were dripped onto C-coated Cu grids, then the solvent is evaporated at room temperature. Nanoparticle size distribution and mean particle size are evaluated with ImageJ software.

4.3 | Electrochemical Measurements

The electrochemical measurements are conducted by using a thermostatic three-electrode electrochemical cell with a rotating disk electrode (RDE, Radiometer Analytical BM-EDI101) equipped with a bipotentiostat Autolab NOVA (PGSTAT302N). Prior to measurement, an open-circuit potential (OCP) test was performed on the as-prepared Pd/C electrode in a continuously N_2-deaerated 0.5 mol L^{-1} H_2SO_4 solution. The measured OCP value was then used as the initial potential for subsequent voltammetry experiments. A glassy carbon disk (0.196 cm^2 geometric SA) and a glassy carbon slab (5 cm^2 geometric SA) are served as working electrode (WE) and counter electrode (CE), respectively. An electrochemically prepared reversible hydrogen electrode (RHE) was used as the reference electrode (RE), connected to the electrochemical cell through a Luggin–Haber capillary to minimize potential drop between the reference and WE. Prior to electrochemical measurements, the glassy carbon electrode was polished by using Al_2O_3 slurry on a synthetic cloth, then rinsed with ultra-pure water and maintained under ultrasonication for 2 min in ethanol.

To prepare the catalytic ink, 490 μL of isopropanol (Sigma Aldrich, 99.5%) and 10 μL Nafion suspension (5 wt.% from Sigma–Aldrich) were ultrasonically mixed for 2 min. Then after a certain amount of catalyst powder (Pd/C, PdCu/C) was added into solvent mixture, yielding a density of 10 μg μL^{-1} homogeneous suspension. Afterwards, a required amount of catalytic ink was gently deposited onto freshly polished WE, yielding a metal loading of 51.0 μg cm^{-2}. The solvent was then evaporated in a stream of ultra-pure N_2 at room temperature for 5 min. All RDE measurements were carried out in an aqueous solution containing 0.5 mol L^{-1} H_2SO_4 (96% from Merck) as supporting electrolyte. Before each CV measurement, the electrolyte was deoxygenated by bubbling nitrogen for 15 min. The EASA was evaluated by integrating the reduction peak of palladium oxide (PdO), which has a charge density of 424 μC cm^{-2} ($Q_{monolayer}$) [56]. The ORR polarization curves were measured using linear scan voltammetry (LSV) with a scan rate of 5 mV s^{-1} and recorded at different rotation rates (200, 400, 625, 900, 1225, 1600, 2025, and 2500 rpm) in O_2-saturated supporting electrolyte. To avoid the risk of chemical and physical contamination, all glassware is meticulously cleaned using concentrated potassium permanganate and piranha solution prior to electrochemical measurements, following procedures described elsewhere [56].

4.4 | PEM Fuel Cell Measurements

For the both catalyst layers are assembled with the total metal loadings of 0.4 mg cm^{-2} for anode (Pt/C 20 wt.%, E-TEK) and cathode (Pd/C or Pd-Cu/C prepared by microwave-heated polyol method). To prepare the catalytic ink, the required amount of catalyst powder (10 mg) is mixed with the Nafion solution (128 μL) and isopropanol (2 mL), and maintained by ultrasonication for 20 min. In all cases, 35 wt.% of Nafion ionomer was incorporated to the catalyst layer by using a Nafion solution (5 wt.% in isopropanol, DuPont). In all cases, 35 wt. % of Nafion (5 wt.% solution in a mixture of alcohols, DuPont) is applied to the catalyst layer. The gas diffusion layer (GDL) consisted of carbon powder (Vulcan XC-72R, Cabot) with 15 (w/w) polytetrafluoroethylene (PTFE, TE-306A, DuPont) deposited onto a carbon cloth substrate (ETEK). The precursor catalytic layer ink is applied directly onto GDL to form the resulting gas diffusion electrodes (GDE). It is critical to handle a pretreatment of Nafion membrane that provides enhanced proton conductivity, ensures proper hydration, reducies interfacial resistance, and removes impurities to achieve optimal stack performance. Thus, Nafion membranes (115, 127 μm, DuPont) are treated in hydrogen peroxide solution (3% v/v) at 80°C for 1 hr followed by rinsing with ultrapure water at same conditions to remove organic traces. Subsequently, the membranes are treated with sulfuric acid solution (0.5 mol.L^{-1}) at 80°C for 1 hr to provide Nafion-H^+-form membranes The MEAs are fabricated by hot pressing the anode and the cathode to the pretreated Nafion 115-based membranes at 125°C and 1000 kgf cm^{-2} for 2 min. Fuel cell polarization measurements are carried out galvanostatically with a 5 cm^2 single cell (Electrocell, Brazil) with serpentine flow pattern. Fuel cells are fed with hydrogen (99.999%) and oxygen (99.998%) at the flow rates of 440 mL min^{-1} and 380 mL min^{-1}, respectively. The gases are saturated with water by using gas humidifiers set to 95°C for H_2 and 85°C for O_2. Herein, the fuel cell test protocol used employs H_2 and O_2 humidification temperatures set at 15°C and 5 °C above the cell temperature, respectively, in order to minimize water management effects on the polarization response and ensure an optimized performance. The polarization curves are recorded at a cell temperature of 80°C under atmospheric pressure. To this end, a standard procedure is considered [82]. Prior to the acquisition of polarization curves, the system is held at 0.7 V for 2 hr to reach steady-state condition. Polarization curves are then recorded by applying current values ranging from 0.01 to 12 A, with step increments between 0.01 and 0.5 A. Each current step is held for 10 s in an ascending scan. Fuel cell tests were conducted by acquiring successive polarization curves until the last two overlapped, indicating system stabilization. The final polarization curve is used for graphical representation, with reproducibility assessed by testing at least two identical MEAs until reproducible results are obtained.

Author Contributions

Roberta A. Isidoro: data curation (lead), formal analysis (lead), investigation (lead), methodology (equal), validation (lead), visualization (supporting), writing – review & editing (supporting). **Nihat E. Şahin**: data curation (lead), formal analysis (equal), investigation (equal), methodology (lead), validation (supporting), visualization (lead), writing original draft (lead). **Fabio C. Fonseca**: funding acquisition (supporting), investigation (supporting), project administration (equal), resources (equal), software (equal), supervision (equal), validation (supporting), writing – review & editing (supporting). **Teko W. Napporn**: conceptualization (lead), data curation (supporting), investigation (supporting), methodology (lead), resources (equal), software (equal), supervision (lead),

2199692x, 2026, 1, Downloaded from https://acces.onlinelibrary.wiley.com/doi/10.1002/cnma.202500324 by University Of Sao Paulo - Brazil, Wiley Online Library on [02/04/2026]. See the Terms and Conditions (https://onlinelibrary.wiley.com/terms-and-conditions) on Wiley Online Library for rules of use; OA articles are governed by the applicable Creative Commons License

validation (supporting), visualization (supporting), writing – review & editing (supporting). **Elisabete I. Santiago**: conceptualization (lead), funding acquisition (lead), methodology (supporting), project administration (equal), resources (equal), software (equal), supervision (lead), validation (supporting), writing – review & editing (supporting). **Kouakou Boniface Kokoh**: conceptualization (lead), funding acquisition (equal), investigation (lead), methodology (lead), project administration (lead), resources (lead), software (equal), supervision (lead), validation (lead), writing – review & editing (supporting).

Acknowledgments

The authors would like to thank the support of the Brazilian agencies CNEN, CAPES, CNPq (Sis-H2 407967/2022−2 and IBH2-MCTI No. 405793/2022−7), and FAPESP (2023/14931−8). FCF and EIS are CNPq fellows. The authors are thankful for the support of the "Region Poitou-Charentes" Council in France for their financial support. N.E.Ş. would like to express his appreciation to Aarhus University for providing the time to prepare this manuscript. This work is part of the French government program "Investissements d'Avenir" (EUR INTREE, reference ANR-18-EURE-0010). Prof. K.B. Kokoh is also grateful to the "Fondation Poitiers Université." and EDF for their financial support (R-2024−37) within his green chemistry projects.

Funding

This work was supported by the Université de Poitiers (R-2024−37); Investissements d'Avenir (EUR INTREE) (ANR-18-EURE-0010); Region Poitou-Charentes (2023/14931−8); FAPESP (2023/14931−8); CNEN, CAPES, CNPq (Sis-H2 407967/2022−2 and IBH2-MCTI No. 405793/2022−7).

Conflicts of Interest

The authors declare no conflicts of interest.

Data Availability Statement

The authors confirm that the data supporting the findings of this study are available within the article.

References

1. X. Zhu, Z. Hu, H. Liu, et al., "Low-Temperature Characteristics and Optimization of the Proton Exchange Membrane Fuel Cells With Anode Ejector," *International Journal of Hydrogen Energy* 109 (2025): 753.

2. F. Zhang, B. Zu, B. Wang, et al., "Developing Long-Durability Proton-Exchange Membrane Fuel Cells," *Joule* 9 (2025): 101853.

3. B. Narayanamoorthy, K. K. R. Datta, and S. Balaji, "Kinetics and Mechanism of Electrochemical Oxygen Reduction Using Platinum/Clay/Nafion Catalyst Layer for Polymer Electrolyte Membrane Fuel Cells," *Journal of Colloid and Interface Science* 387 (2012): 213.

4. D. C. Martínez-Casillas, G. Vázquez-Huerta, J. F. Pérez-Robles, and O. Solorza-Feria, "Electrocatalytic Reduction of Dioxygen on PdCu for Polymer Electrolyte Membrane Fuel Cells," *Journal of Power Sources* 196 (2011): 4468.

5. T. Inoue, T. Uma, and M. Nogami, "Performance of H_2/O_2 Fuel Cell Using Membrane Electrolyte of Phosphotungstic Acid-Modified 3-Glycidoxypropyl-Trimethoxysilanes," *Journal of Membrane Science* 323 (2008): 148.

6. N. C. Ereli, M. Kıstı, T. Eşiyok, et al., "First Pulsed Control System Design for Enhanced Hydrogen Production Performance in Proton Exchange Membrane Water Electrolyzers," *Fuel* 371 (2024): 132027.

7. U. A. Paulus, A. Wokaun, G. G. Scherer, et al., "Oxygen Reduction on Carbon-Supported Pt-Ni and Pt-Co Alloy Catalysts," *The Journal of Physical Chemistry B* 106 (2002): 4181.

8. Y. Holade, N. E. Sahin, K. Servat, T. Napporn, and K. Kokoh, "Recent Advances in Carbon Supported Metal Nanoparticles Preparation for Oxygen Reduction Reaction in Low Temperature Fuel Cells," *Catalysts* 5 (2015): 310.

9. H. A. Gasteiger, S. S. Kocha, B. Sompalli, and F. T. Wagner, "Activity Benchmarks and Requirements for Pt, Pt-Alloy, and Non-Pt Oxygen Reduction Catalysts for PEMFCs," *Applied Catalysis B: Environmental* 56 (2005): 9.

10. F. Xiao and M. Shao, "Electrocatalyst and Electrode Design Strategies for Durable Proton Exchange Membrane Fuel Cells," *Matter* 7 (2024): 351.

11. Y. Tang, H. Zhang, H. Zhong, and Y. Ma, "A Facile Synthesis of Pd/C Cathode Electrocatalyst for Proton Exchange Membrane Fuel Cells," *International Journal of Hydrogen Energy* 36 (2011): 725.

12. S. A. Grigoriev, E. K. Lyutikova, S. Martemianov, and V. N. Fateev, "On the Possibility of Replacement of Pt by Pd in a Hydrogen Electrode of PEM Fuel Cells," *International Journal of Hydrogen Energy* 32 (2007): 4438.

13. Z. A. Che Ramli, J. Pasupuleti, N. F. H. Nik Zaiman, et al., "Evaluating Electrocatalytic Activities of Pt, Pd, Au and Ag Based Catalyst on PEMFC Performance: A Review," *International Journal of Hydrogen Energy* 104 (2025): 463.

14. J. Moreira, P. del Angel, A. L. Ocampo, P. J. Sebastián, J. A. Montoya, and R. H. Castellanos, "Synthesis, Characterization and Application of a Pd/Vulcan and Pd/C Catalyst in a PEM Fuel Cell," *International Journal of Hydrogen Energy* 29 (2004): 915.

15. S. Salomé, R. Rego, A. Querejeta, F. Alcaide, and M. C. Oliveira, "An Electrochemical Route to Prepare Pd Nanostructures on a Gas Diffusion Substrate for a PEMFC," *Electrochimica Acta* 106 (2013): 516.

16. O. Savadogo, K. Lee, K. Oishi, S. Mitsushima, N. Kamiya, and K. I. Ota, "New Palladium Alloys Catalyst for the Oxygen Reduction Reaction in an Acid Medium," *Electrochemistry Communications* 6 (2004): 105.

17. S. Nogami, N. Shida, S. Iguchi, et al., "Mechanistic Insights into the Electrocatalytic Hydrogenation of Alkynes on Pt Pd Electrocatalysts in a Proton Exchange Membrane Reactor," *ACS Catalysis* 12 (2022): 5430.

18. V. Raghuveer, A. Manthiram, and A. J. Bard, "Pd-Co-Mo Electrocatalyst for the Oxygen Reduction Reaction in Proton Exchange Membrane Fuel Cells," *The Journal of Physical Chemistry B* 109 (2005): 22909.

19. V. Raghuveer, P. J. Ferreira, and A. Manthiram, "Comparison of Pd–Co–Au Electrocatalysts Prepared by Conventional Borohydride and Microemulsion Methods for Oxygen Reduction in Fuel Cells," *Electrochemistry Communications* 8 (2006): 807.

20. D. C. Martínez-Casillas, H. A. Calderon, V. Collins-Martínez, and O. Solorza-Feria, "Pd_5Cu_4Pt Oxygen Reduction Nanocatalyst for PEM Fuel Cells," *International Journal of Hydrogen Energy* 38 (2013): 12674.

21. S. M. Senthil Kumar, J. Soler Herrero, S. Irusta, and K. Scott, "The Effect of Pretreatment of Vulcan XC 72R Carbon on Morphology and Electrochemical Oxygen Reduction Kinetics of Supported Pd Nanoparticle in Acidic Electrolyte," *Journal of Electroanalytical Chemistry* 647 (2010): 211.

22. S. Han, C. He, Q. Yun, et al., "Pd Based Intermetallic Nanocrystals: From Precise Synthesis to Electrocatalytic Applications in Fuel Cells," *Coordination Chemistry Reviews* 445 (2021): 214085.

23. W. Baek, H. Chang, M. S. Bootharaju, J. H. Kim, S. Park, and T. Hyeon, "Recent Advances and Prospects in Colloidal Nanomaterials," *JACS Au* 1, no. 11 (2021): 1849.

24. N. Sahin, W. O. Silva, M. R. Camilo, et al., "CO_2 Electroreduction to Fuels on Mesoporous Carbon Embedded Copper Nanoparticles," *Sustainable Energy Fuels* 4 (2020): 6045.

2199692x, 2026, 1, Downloaded from https://acces.onlinelibrary.wiley.com/doi/10.1002/cnma.202500324 by University Of Sao Paulo - Brazil, Wiley Online Library on [02/04/2026]. See the Terms and Conditions (https://onlinelibrary.wiley.com/terms-and-conditions) on Wiley Online Library for rules of use; OA articles are governed by the applicable Creative Commons License

25. A. Heuer-Jungemann, N. Feliu, I. Bakaimi, et al., "The Role of Ligands in the Chemical Synthesis and Applications of Inorganic Nanoparticles," *Chemical Reviews* 119 (2019): 4819.

26. R. Gedye, F. Smith, K. Westaway, et al., "The Use of Microwave Ovens for Rapid Organic Synthesis," *Tetrahedron Letters* 27 (1986): 279.

27. R. J. Giguere, T. L. Bray, S. M. Duncan, and G. Majetich, "Application of Commercial Microwave Ovens to Organic Synthesis," *Tetrahedron Letters* 27 (1986): 4945.

28. F. Fievet, J. P. Lagier, B. Blin, B. Beaudoin, and M. Figlarz, "Homogeneous and Heterogeneous Nucleations in the Polyol Process for the Preparation of Micron and Submicron Size Metal Particles," *Solid State Ionics* 32-33 (1989): 198.

29. W. J. Pech-Rodríguez, H. M. García-Lezama, and N. E. Sahin, "Facile Preparation of SnO_2/CuO Nanocomposites as Electrocatalysts for Energy Efficient Hybrid Water Electrolysis in the Presence of Ethanol," *Energies* 16 (2023): 4986.

30. R. J. Joseyphus, D. Kodama, T. Matsumoto, Y. Sato, B. Jeyadevan, and K. Tohji, "Role of Polyol in the Synthesis of Fe Particles," *Journal of Magnetism and Magnetic Materials* 310 (2007): 2393.

31. N. E. Şahin, C. Comminges, S. Arrii, T. W. Napporn, and K. B. Kokoh, "CO_2 to HCOOH Electrochemical Conversion on Nanostructured Cu_xPd_{100-x}/Carbon Catalysts," *ChemElectroChem* 8 (2021): 1362.

32. N. T. N. Hang, Y. Yang, L. H. Phuc, N. H. Tri, H. V. Cuu, and N. V. Long, "Shape-Controlled Synthesis of Micro-/Nanosized Cu Particles With Spherical and Polyhedral Shapes Using the Polyol Process," *RSC Advances* 14 (2024): 22403.

33. S. Karadeniz and N. Ayas, "Microwave Assisted Synthesis of Pt/C Catalyst at High Temperatures for PEM Fuel Cells," *International Journal of Hydrogen Energy* 52 (2024): 1564.

34. P. Chattopadhyay, T. Gemming, A. Eychmuller, and J. Simmchen, "Polyol-Assisted Synthesis of Copper Particles," *The Journal of Physical Chemistry C* 125 (2021): 24887.

35. J.-Y. Kim, K.-H. Kim, S.-H. Park, and K.-B. Kim, "Microwave Polyol Synthesis of Nanocrystalline Ruthenium Oxide Nanoparticles on Carbon Nanotubes for Electrochemical Capacitors," *Electrochimica Acta* 55 (2010): 8056.

36. Q. Shu, S. Yang, X. Zhang, et al., "A systematic investigation on the effects of Cu^{2+} Contamination on the Performances and Durability of Proton Exchange Membrane Fuel Cells," *International Journal of Hydrogen Energy* 57 (2024): 90.

37. S. Moorthy, R. Sudhakaran, A. Mahalingam, H. Pushparaj, and P. Deivanayagam, "Enhancing Fuel Cell Erformance: The Role of a Copper Metal–Organic Framework in Phosphoric Acid Doped Polybenzimidazole Proton Exchange Membranes," *Industrial & Engineering Chemistry Research* 63 (2024): 17567.

38. N. A. B. Johnson, S. K. Das, and A. K. Sen, "Effects of Copper Corrosion in the Performance of Polymer Electrolyte Membrane Fuel Cells," *ECS Transactions* 80, no. 8 (2017): 477.

39. L. Mølmen, K. Eiler, L. Fast, P. Leisner, and E. Pellicer, "RRecent Advances in Catalyst Materials for Proton Exchange Membrane Fuel Cells," *APL Matter* 9 (2021): 040702.

40. L. Vichard, R. Petrone, F. Harel, A. Ravey, P. Venet, and D. Hissel, "Long-Term Durability Test of Open-Cathode Fuel Cell System Under Actual Operating Conditions," *Energy Conversion and Management* 212 (2020): 112813.

41. S. R. Krishnan, D. Verstraete, and F. Aguey-Zinsou, "Performance of Non-Precious Metal Electrocatalysts in Proton-Exchange Membrane Fuel Cells: A Review," *ChemElectroChem* 11 (2024): e202400299.

42. B. J. Kim, S. H. Park, M. L. Diaz-Ramirez, and N. C. Jeong, "Proton-Conducting Copper-Based MOFs for Fuel Cells," *Chemical Communications* 61 (2025): 3582.

43. S. G. Peera, C. Liu, A. Asokan, and M. E. Suss, "Cu@NC as High-Performance and Durable Electrocatalyst for Oxygen Reduction Reaction in Alkaline Membrane Fuel Cells," *Journal of Alloys and Compounds* 938 (2023): 168636.

44. H. Liu, X. Zong, Y. Wang, Z. Hu, and Z. Zhang, "MOF-Derived CoP/CuP Hybrids as Bifunctional Electrocatalysts for Zinc–Air Batteries," *New Journal of Chemistry* 48 (2024): 9534.

45. L. Castanheira, L. Dubau, M. Mermoux, et al., "Carbon Corrosion in Proton Exchange Membrane Fuel Cells: From Model Experiments to Real Life Operation in Membrane Electrode Assemblies," *ACS Catalysis* 4 (2014): 2258.

46. M. Lu, J. Liang, W. Zhang, et al., "CCorrosion Mechanism and Mitigation Strategies for Carbon Supports in PEMFCs," *Advanced Sustainable Systems* (2024): 2400742, https://doi.org/10.1002/adsu.202400742.

47. F. Hegge, J. Sharman, R. Moroni, et al., "Impact of Carbon Support Corrosion on Performance Losses in Polymer Electrolyte Membrane Fuel Cells," *Journal of the Electrochemical Society* 166 (2019): F956.

48. X. Cai, X. Liu, X. Wie, and R. Lin, "Effect of Nitrogen Doped Carbon Materials in Electrocatalysis," *ACS Applied Energy Materials* 7 (2024): 8705.

49. A. Gashi, J. Parmentier, P. Fioux, and R. Marsalek, "Tuning the C/N Ratio of C-Rich Graphitic Carbon Nitride ($g\text{-}C_3N_4$) Materials by the Melamine/Carboxylic Acid Adduct Route," *Chemistry: A European Journal* 28 (2022): e202103605.

50. Y. Holade, C. Morais, K. Servat, T. W. Napporn, and K. B. Kokoh, "Enhancing the Available Specific Surface Area of Carbon Supports to Boost the Electroactivity of Nanostructured Pt Catalysts," *Physical Chemistry Chemical Physics* 16 (2014): 25609.

51. V. Sinha, F. Rezai, N. E. Sahin, et al., "Electrochemical Nitrogen Reduction Reaction Over Gallium–A Computational and Experimental Study," *Faraday Discussions* 243 (2023): 307.

52. X. Wang, N. Kariuki, J. T. Vaughey, J. Goodpaster, R. Kumar, and D. J. Myers, "Bimetallic Pd–Cu Oxygen Reduction Electrocatalysts," *Journal of the Electrochemical Society* 155 (2008): B602.

53. H. Zhang, Q. Hao, H. Geng, and C. Xu, "Nanoporous PdCu Alloys as Highly Active and Methanol Tolerant Oxygen Reduction Electrocatalysts," *International Journal of Hydrogen Energy* 38 (2013): 10029.

54. N. Tateishi, K. Yahikozawa, K. Nishimura, and Y. Takasu, "Hydrogen Electrode Reaction on Electrodes of Glassy Carbon," *Electrochimica Acta* 37, no. 13 (1992): 2427.

55. D. Diabaté, T. W. Napporn, K. Servat, et al., "Kinetic Study of Oxygen Reduction Reaction on Carbon Supported Pd Based Nanomaterials in Alkaline Medium," *Journal of the Electrochemical Society* 160 (2013): H302.

56. N. E. Şahin and W. J. Pech-Rodríguez, "Scrutinizing the Basis of Pd Electrochemistry: An Accurate Assessment of the Electrochemically Active Surface Area," *Electroanalysis* 37 (2025): e12027.

57. Y. Holade, R. G. da Silva, K. Servat, et al., "Facile Synthesis of Highly Active and Durable PdM/C (M = Fe, Mn) Nanocatalysts for the Oxygen Reduction Reaction in an Alkaline Medium," *Journal of Materials Chemistry A* 4 (2016): 8337.

58. R. K. Singh, R. Devivaraprasad, T. Kar, A. Chakraborty, and M. Neergat, "Electrochemical Impedance Spectroscopy of Oxygen Reduction Reaction (ORR) in a Rotating Disk Electrode Configuration: Effect of Ionomer Content and Carbon Support," *Journal of the Electrochemical Society* 162 (2015): F489.

59. N. E. Sahin, T. W. Napporn, L. Dubau, F. Kadirgan, J.-M. Leger, and K. B. Kokoh, "Temperature-Dependence of Oxygen Reduction Activity on Pt/C and PtCr/C Electrocatalysts Synthesized from Microwave-Heated

21996892x, 2026, 1, Downloaded from https://acces.onlinelibrary.wiley.com/doi/10.1002/cnma.202500324 by University Of Sao Paulo - Brazil, Wiley Online Library on [02/04/2026]. See the Terms and Conditions (https://onlinelibrary.wiley.com/terms-and-conditions) on Wiley Online Library for rules of use; OA articles are governed by the applicable Creative Commons License

Diethylene Glycol Method," *Applied Catalysis B: Environmental* 203 (2017): 72.

60. S. Xu, Y. Kim, D. Higgins, M. Yusuf, T. F. Jaramillo, and F. B. Prinz, "Building Upon the Koutecký-Levich Equation for Evaluation of Next-Generation Oxygen Reduction Reaction Catalysts," *Electrochimica Acta* 255 (2017): 99.

61. K. E. Gubbins and R. D. Walker, "The Solubility and Diffusivity of Oxygen in Electrolytic Solutions," *Journal of the Electrochemical Society* 112 (1965): 469.

62. S. K. Zecevic, J. S. Wainright, M. H. Litt, S. L. Gojkovic, and R. F. Savinell, "Kinetics of O_2 Reduction on a Pt Electrode Covered with a Thin Film of Solid Polymer Electrolyte," *Journal of the Electrochemical Society* 144 (1997): 2973.

63. C. Coutanceau, M. J. Croissant, T. Napporn, and C. Lamy, "Electrocatalytic reduction of dioxygen at platinum particles dispersed in a polyaniline film," *Electrochimica Acta* 46 (2000): 579.

64. D. B. Sepa, M. V. Vojnovic, L. M. Vracar, and A. Damjanovic, "Apparent Enthalpies of Activation of Electrodic Oxygen Reduction at Platinum in Different Current-Density Regions," *Electrochimica Acta* 31 (1986): 91.

65. H. Erikson, M. Liik, A. Sarapuu, J. Kozlova, V. Sammelselg, and K. Tammeveski, "Oxygen Reduction on Electrodeposited Pd Coatings on Glassy Carbon," *Electrochimica Acta* 88 (2013): 513.

66. T. Lopes, V. A. Paganin, and E. R. Gonzalez, "Hydrogen Sulfide Tolerance of Palladium–Copper Catalysts for PEM Fuel Cell Anode Applications," *International Journal of Hydrogen Energy* 36 (2011): 13703.

67. M. H. Seo, E. J. Lim, S. M. Choi, S. H. Nam, H. J. Kim, and W. B. Kim, "Synthesis, Characterization, and Electrocatalytic Properties of a Polypyrrole-Composited Pd/C Catalyst," *International Journal of Hydrogen Energy* 36 (2011): 11545.

68. J. H. Ozdemir, A. Hasimoglu, H. Elcicek, O. K. Ozdemir, and N. Akkas, "Production of highly efficient Pt/C for PEM fuel cell applications," *Electrocatalysis* 16 (2025): 379.

69. F. Fouda-Onana, S. Bah, and O. Savadogo, "Palladium–Copper Alloys as Catalysts for the Oxygen Reduction Reaction in an Acidic Medium I: Correlation Between the ORR Kinetic Parameters and Intrinsic Physical Properties of the Alloys," *Journal of Electroanalytical Chemistry* 636 (2009): 1–9.

70. A. J. Medford, A. Vojvodic, J. S. Hummelshøj, et al., "From the Sabatier Principle to a Predictive Theory of Transition-Metal Heterogeneous Catalysis," *Journal of Catalysis* 328 (2015): 36.

71. K. Li, Z. Tao, X. Ma, et al., "The Application and Research Progress of d-Band Center Theory in the Field of Water Electrolysis," *International Journal of Hydrogen Energy* 132 (2025): 183.

72. W. Zhang, S. Shan, J. Luo, et al., "Origin of Enhanced Activities for CO Oxidation and O_2 Reaction Over PdCu Alloy Nanoparticles," *The Journal of Physical Chemistry C* 121 (2017): 11010.

73. H. Huang, Y. Chen, H. Fu, et al., "d-d Orbital Coupling Induced by Crystal-Phase Engineering Toward High-Performance Electrocatalysis," *Journal of Energy Chemistry* 89 (2024): 216.

74. V. Sanchez-Escribano, L. Arrighi, P. Riani, R. Marazza, and G. Busca, "Characterization of Pd–Cu Alloy Nanoparticles on γ-Al_2O_3-Supported Catalysts," *Langmuir* 22 (2006): 9214.

75. X. Nie, X. Jiang, H. Wang, et al., "Mechanistic Understanding of Alloy Effect and Water Promotion for Pd Cu Bimetallic Catalysts in CO_2 Hydrogenation to Methanol," *ACS Catalysis* 8 (2018): 4873.

76. X. Jiang, Y. Jiao, C. Moran, et al., "CO_2 Hydrogenation to Methanol on Pd–Cu Bimetallic Catalysts with Lower Metal Loadings," *Catalysis Communications* 118 (2019): 10.

77. K. I. Choi and M. A. Vannice, "CO Oxidation Over Pd and Cu Catalysts. V. Al_2O_3-Supported Bimetallic Pd-Cu Particles," *Journal of Catalysis* 131 (1991): 36.

78. Y. Jiang, A. M. H. Lim, H. Yan, H. C.Zeng, and U. Mirsaidov, "Phase Segregation in PdCu Alloy Nanoparticles During CO Oxidation Reaction at Atmospheric Pressure," *Advanced Science* 10 (2023): 2302663.

79. J. Xue, G. Han, W. Ye, et al., "Structural Regulation of $PdCu_2$ Nanoparticles and their Electrocatalytic Performance for Ethanol Oxidation," *ACS Applied Materials & Interfaces* 8 (2016): 34497.

80. C. F. Holder and R. E. Schaak, "Tutorial on Powder X-Ray Diffraction for Characterizing Nanoscale Materials," *ACS Nano* 13 (2019): 7359.

81. M. F. Perutz, "Sir Lawrence Bragg," *Acta Crystallographica. Section A, Foundations of Crystallography* 69 (2013): 8.

82. L. P. R. Moraes, B. R. Matos, C. Radtke, et al., "Synthesis and Performance of Palladium-Based Electrocatalysts in Alkaline Direct Ethanol Fuel Cell," *International Journal of Hydrogen Energy* 41, no.15, (2016): 6457.

Supporting Information

Additional supporting information can be found online in the Supporting Information section. **Supporting Fig. S1:** (a) Typical polarization curves recorded at different rotation rates and scan rate of 5 mV s^{-1} in an O_2-saturated 0.5 M H_2SO_4 electrolyte for $Pd_{90}Cu_{10}$/C electrocatalyst, (b) related Koutecký-Levich plots determined at different potentials from 0.80 to 0.70 V vs. RHE, (c) Plot of 1/jk as a function of the applied potential and (d) related Tafel plots for low over potential and high over potential regions. The total metal loading on the electrode: 51 μg cm^{-2}. **Supporting Fig. S2:** (a) Typical polarization curves recorded at different rotation rates and scan rate of 5 mV s^{-1} in an O_2-saturated 0.5 M H_2SO_4 electrolyte for $Pd_{70}Cu_{30}$/C electrocatalyst, (b) related Koutecký-Levich plots determined at different potentials from 0.80 to 0.70 V vs. RHE, (c) Plot of 1/jk as a function of the applied potential and (d) related Tafel plots for low over potential and high over potential regions. The total metal loading on the electrode: 51 μg cm^{-2}. **Supporting Fig. S3:** (a) Typical polarization curves recorded at different rotation rates and scan rate of 5 mV s^{-1} in an O_2-saturated 0.5 M H_2SO_4 electrolyte for $Pd_{50}Cu_{50}$/C electrocatalyst, (b) related Koutecký-Levich plots determined at different potentials from 0.80 to 0.70 V vs. RHE, (c) Plot of 1/jk as a function of the applied potential and (d) related Tafel plots for low over potential and high over potential regions. The total metal loading on the electrode: 51 μg cm^{-2}.

Biographies

Roberta A. Isidoro is a professor of chemistry at Faculdades Oswaldo Cruz in São Paulo, Brazil. She obtained her Ph.D. in materials science in 2015 from IPEN, the Institute for Energy and Nuclear Research, during which she collaborated with the IC2MP Electrocatalysis Research Group at the Université de Poitiers in France. Her research focuses on the development and characterization of nanomaterials, composite membranes for direct ethanol fuel cells, and the improvement of electrocatalysts for low-temperature fuel cell applications. She also investigates and optimizes fuel cell key components to enhance energy efficiency.

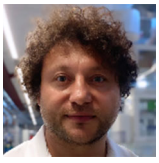

Nihat E. Şahin's research focuses on the development and optimization of electrochemical processes and instrumentation for applications in batteries, fuel cells, and electrolyzers. He specialized in electrode dynamics and hydrodynamic voltammetry for ORR/OER at Istanbul Technical University (Türkiye). He then obtained his Ph.D. (2016) from the University of Poitiers (France) under the supervision of Prof. Boniface Kokoh, where his work was firmly rooted on the synthesis and microstructural characterization of nanomaterials for HER and CO_2 electroreduction, along with electrochemical system integration. Recently, Dr. Şahin has been focusing on electrochemical ammonia synthesis and stationary batteries as a postdoctoral researcher at Aarhus University (Denmark).

2199692x, 2026, 1, Downloaded from https://acces.onlinelibrary.wiley.com/doi/10.1002/cnma.202500324 by University Of Sao Paulo - Brazil, Wiley Online Library on [02/04/2026]. See the Terms and Conditions (https://onlinelibrary.wiley.com/terms-and-conditions) on Wiley Online Library for rules of use; OA articles are governed by the applicable Creative Commons License

Fabio C. Fonseca's research focuses on materials for sustainable energy, with an emphasis on electroceramics. He is a senior researcher and the head of the Fuel Cell and Hydrogen Center at the Nuclear and Energy Research Institute (IPEN) in São Paulo, Brazil. At IPEN he is the principal investigator of research projects to expand power-to-X technologies using sustainable fuels such as ethanol and biomethane, with several collaborators, funding agencies, and companies.

Teko W. Napporn is a Director of Research at the French National Center for Scientific Research (CNRS) at the University of Poitiers. After obtaining his Ph.D. in 1997 at the University of Poitiers, he joined the Institute of Chemistry of Sao Carlos (USP, Brazil) as a postdoctoral fellow and in 1999 the Ecole Polytechnique de Montreal (Canada) as a Research Associate. There, he had developed the single chamber SOFC system in collaboration with Hydro-Quebec. Since 2008, he has been developing at IC2MP (University of Poitiers), novel electrode nanomaterials for energy conversion and storage systems such as low temperature fuel cells and electrolysis of water and biomass. Since September 2015, he has been an adjunct professor at the Institute of Advanced Sciences at Yokohama National University in Japan.

Elisabete I. Santiago is a senior researcher at the Nuclear and Energy Research Institute (IPEN) in São Paulo, Brazil. Her background is in electrochemistry, with a focus on new energy technologies such as fuel cells, electrolysis, and the electrochemical conversion of methane and carbon dioxide into value-added compounds. Recently, she has been dedicated to the development of a new generation of anion-exchange membranes (AEMs) produced via radiation-induced grafting.

Kouakou Boniface Kokoh is a full professor of electrocatalysis at Université de Poitiers (France). His research interests involve hydrogen production in a solid polymer electrolyte water electrolyzer, abiotic electrode design for hybrid (bio)-fuel cells and the CO_2 electroreduction to platform molecules. His research also focuses on HER/HOR and ORR/OER, nanomaterial synthesis, and characterizations.

2199692x, 2026, 1, Downloaded from https://acces.onlinelibrary.wiley.com/doi/10.1002/cnma.202500324 by University Of Sao Paulo - Brazil, Wiley Online Library on [02/04/2026]. See the Terms and Conditions (https://onlinelibrary.wiley.com/terms-and-conditions) on Wiley Online Library for rules of use; OA articles are governed by the applicable Creative Commons License